AIP | Applied Physics Letters

Optical properties of Bi 3.15 Nd 0.85 Ti 3 O 12 nanostructures

Wei Cai, Xiaomei Lu, De Li, Huifeng Bo, Ruwen Peng, Xiaobo Wu, Yunfei Liu, and Jinsong Zhu

Citation: Applied Physics Letters **94**, 092906 (2009); doi: 10.1063/1.3095666
View online: http://dx.doi.org/10.1063/1.3095666
View Table of Contents: http://scitation.aip.org/content/aip/journal/apl/94/9?ver=pdfcov
Published by the AIP Publishing

Optical properties of $Bi_{3.15}Nd_{0.85}Ti_3O_{12}$ nanostructures

Wei Cai, Xiaomei Lu,[a] De Li, Huifeng Bo, Ruwen Peng, Xiaobo Wu, Yunfei Liu, and Jinsong Zhu

Physics Department, National Laboratory of Solid State Microstructures, Nanjing University, Nanjing 210093, People's Republic of China

(Received 16 January 2009; accepted 12 February 2009; published online 6 March 2009)

Ferroelectric materials are widely researched because of their application in electronic devices. A ferroelectric nanotube is important both theoretically and experimentally because of its nonplanar structure. $Bi_{3.15}Nd_{0.85}Ti_3O_{12}$ nanotubes are fabricated utilizing templates of porous anodic aluminum oxide and thin films are synthesized as well for comparison. Atomic force microscopy, scanning electron microscopy, and x-ray diffraction reveal the microstructure of the samples. The optical properties are investigated carefully to reveal the size effect with the decrease in sample dimensionality. The observed shift of the absorption edge for different nanostructures is discussed. © *2009 American Institute of Physics*. [DOI: 10.1063/1.3095666]

Ferroelectrics have been widely researched because of their potential applications in actuators, transducers, and nonvolatile memories.[1,2] Recent years, more and more attention has been paid to nanometric ferroelectrics from thin films to nanowires and nanotubes because of their probability in greatly improving the storage density of ferroelectric random access memory.[3–8] It is known that nanoscale materials exhibit different characteristics such as magnetic, electrical, and optical properties[9,10] from their bulk form as a result of the lower dimensionality and larger aspect ratio. Furthermore, it is of great importance to research the size limit of ferroelectricity,[11,12] which is known as the ferroelectricity fading away when the scale gets down to a certain limit.

The nanostructure of the ferroelectric perovskites, $BaTiO_3$,[8] and lead zirconate titanate[13] has been intensively studied. However, few works have been reported on the nanostructure (especially nanotubes) of Bi-layered perovskites, another most attractive ferroelectrics for their lead free and fatigue free characteristics, with the work by Morrison *et al.*[5] as the earliest report on this subject. To our consideration, the possible reason might be that, in Bi-layered perovskites, the ratio of the two main axes, c/a, is much larger than that of simple perovskites ($BaTiO_3$, $c/a \sim 1$). The big anisotropy might cause increased difficulty in the fabrication of nanoscale Bi-layered perovskites. Actually, a ferroelectric nanotube needs more concern because there exits one more dielectric surface originating from its nonplanar geometry, which is important in the integration of three-dimensional memory devices.[14,15] Here we report the synthesis and characterization of $Bi_{3.15}Nd_{0.85}Ti_3O_{12}$ (BNT) nanotubes. By carefully analyzing and comparing the optical properties of the nanotubes and thin films, we show an interesting shift of absorption edge related with the sample geometry. The results may be helpful for the understanding of size effect on the physical properties of nanoscale materials.

The samples are prepared via sol-gel method. BNT films with different thicknesses are deposited on fused quartz substrates adopting a procedure described before.[16] BNT nanotubes are fabricated via infiltration method utilizing templates of porous anodic aluminum oxide (AAO) with a thickness of 50 μm and a pore diameter of 100 nm.[17] The AAO template is first immersed into the 0.2*M* BNT precursor solution for 12 h, then annealed at different temperatures for 0.5 h in oxygen atmosphere. The microstructures of the samples are characterized by x-ray diffraction (XRD) (D/Max-RB) with Cu $K\alpha$ radiation, an atomic force microscope (AFM) (DI, Nano IV), and a scanning electron microscope (SEM) (Philips, XL-30). The optical properties are studied by a UV/visible/near infrared spectrophotometer (PerkinElmer, Lambda 900).

Figure 1 shows the XRD patterns of BNT films annealed at 700 °C [Fig. 1(a)] and 750 °C [Fig. 1(b)]. All films show the polycrystalline perovskite structure without preferred orientation. The diffraction peaks become sharper and the full width at half maximum decreases as the film thickness and

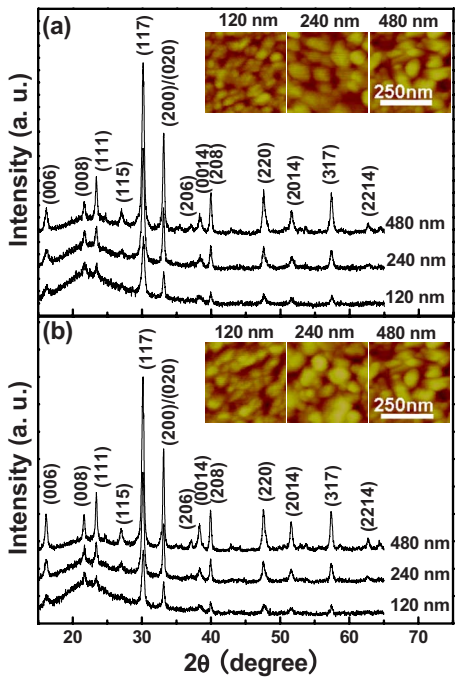

FIG. 1. (Color online) XRD patterns of BNT films deposited on fused quartz substrates annealed at (a) 700 and (b) 750 °C. Insets show the AFM surface morphology of corresponding BNT films with different thicknesses.

[a]FAX: +86-25-8359-5535. Electronic mail: xiaomeil@nju.edu.cn.

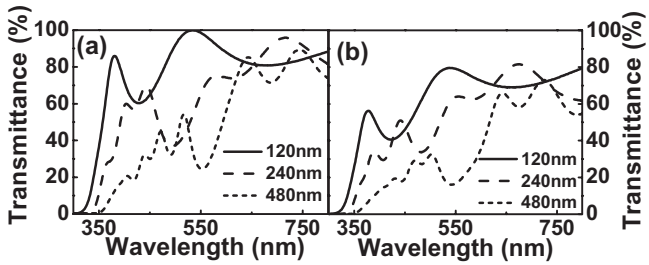

FIG. 2. Optical transmission spectra of (a) 700 and (b) 750 °C annealed BNT films with different thicknesses.

annealing temperature increase, which indicates the increase in grain size. Insets of Fig. 1 show the AFM images of the above samples. The grain size increases obviously with the increase in film thickness and it also increases slightly with the annealing temperature rising from 700 to 750 °C. The AFM observations accord with the XRD result aforementioned. Both the XRD patterns and AFM images can be utilized to estimate the average grain size of the films. The grain size estimated by AFM is usually considered larger than the real situation,[18] while XRD analysis reflects the single crystalline size. Therefore Scherrer's equation[19,20] $L=K\lambda/\beta\cos\theta$ is adopted to estimate the average grain size of the films with the instrumental broadening subtracted, where L is the grain size, λ is the wavelength of the X ray, θ is the diffraction angle, β is the full width at half maximum of the diffraction peak, and K is a constant usually taken as 0.94.

Figure 2 gives the optical transmission spectra of the above samples. For the films annealed at the same temperature, either 700 or 750 °C, the absorption limit shifts obviously to longer wavelength with the increase in film thickness. The absorption edge demonstrates the energy band gap of dielectrics. A more accurate estimate of the bandgap E_g can be made from the graph of $(\alpha h\nu)^2$ against $h\nu$ for the absorption coefficient α is related to the bandgap E_g as $(\alpha h\nu)^2=\text{const.}(h\nu-E_g)$, where $h\nu$ is the energy of incident light.[21]

Table I lists the average grain size and energy band gap of all the BNT films synthesized. It can be seen that the average grain size of 700 °C annealed 120 nm thick BNT film is about 47 nm. Then with the increase in film thickness or annealing temperature, the average grain size gradually increases to about 89 nm at 750 °C and 480 nm thickness. Correspondingly, the energy band gap diminishes from 3.83 to 3.49 eV and becomes closer to 2.8 eV of $Bi_4Ti_3O_{12}$ bulk crystal. The shift in the optical band-gap energy could be

TABLE I. Average grain size and energy band gap of BNT films on quartz substrates.

Annealing temperature (°C)	Film thickness (nm)	Average grain size (nm)	Absorption limit (nm)	E_g (eV)
700	120	47	324	3.83
750	120	54	326	3.81
700	240	59	340	3.65
750	240	69	342	3.63
700	480	78	353	3.52
750	480	89	356	3.49

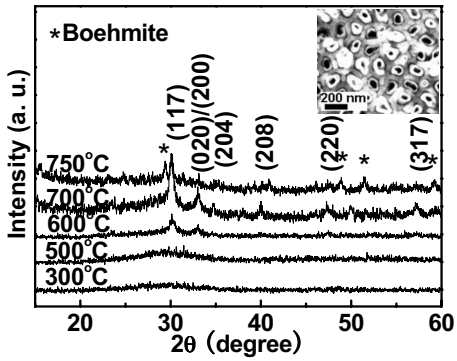

FIG. 3. XRD pattern of BNT nanotube arrays embedded in AAO templates annealed at different temperatures. Inset shows the SEM image of 700 °C annealed BNT nanotubes embedded in AAO template.

explained in terms of quantum size effects.[22] The decrease in sample dimension and in turn the decrease in crystalline integrality results in an obviously increase in energy band gap.

In order to learn more about the change in optical properties with the transformations of dimension and geometry, BNT nanotubes are studied as well. Figure 3 shows the XRD patterns of BNT nanotubes embedded in AAO template annealed at different temperatures. The (117) peak of BNT appears after annealing at 600 °C, which indicates the transformation from the amorphous to Bi-layered perovskite phase. At 700 °C, the intensity of the (117), (020), and (220) peaks of BNT is observably increased. However, when the annealing temperature is elevated to 750 °C, the diffraction peaks of the Boehmite phase of alumina begin to appear. Meanwhile, the (020) and (220) peaks of BNT fade away, which suggests that the alumina participates in the growth of BNT nanotubes when the annealing temperature is above 750 °C. Hence, in the following, the 600 and 700 °C annealed BNT nanotubes are carefully studied.

Inset of Fig. 3 shows the SEM image of 700 °C annealed BNT nanotubes. The open end demonstrates the tubular geometries of BNT. The outer diameter of the nanotubes is about 100 nm and the wall thickness is about 25–30 nm. After the AAO template is completely etched by 0.2*M* NaOH, the BNT nanotubes are distributed in alkaline solution, then centrifugalized and dispersed in de-ionized water. The inset of Fig. 4 shows the optical transmission spectrum of 700 °C annealed BNT nanotubes dispersed in de-ionized water. The transmittance shows a strong drop around 352 nm and the energy band gap is calculated to be 3.53 eV. The

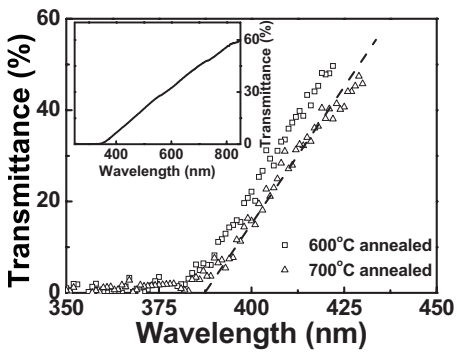

FIG. 4. Optical transmission spectra of 600 and 700 °C annealed BNT nanotubes embedded in AAO templates in the region of strong absorption. Inset shows the transmission spectrum of 700 °C annealed BNT nanotubes dispersed in de-ionized water.

band gap energy of 700 °C annealed BNT nanotubes in de-ionized water is close to that of the 480-nm-thick BNT film (Table I), although the grain size of the former (~28 nm) is much smaller than that of the latter (~78 nm). The "inconsistency" might be related to the nanoscale tubular geometry of BNT nanotubes. XRD analysis reveals the average grain size in the lateral direction of the nanotubes. When the nanotubes are dispersed in de-ionized water, the effective grain size along the direction of the incident light might be larger. An interesting phenomenon is that, when the nanotubes are embedded in the AAO template, the energy band gap shifts even further to the lower energy. As shown in Fig. 4, the transmittance of the 600 and 700 °C annealed nanotube samples drops at 382 and 388 nm, respectively. The band gap energy of 700 °C annealed BNT nanotubes in AAO template is estimated to be only 3.20 eV. The variation in energy band gap between 700 °C annealed BNT nanotubes in different media is probably due to the different alignments of the nanotubes. The nanotubes are randomly distributed in de-ionized water while it aligns regularly in the AAO template. When the light is along the normal direction of the template, it actually propagates through a two-dimensional periodic array with about 200 nm periodicity and 50 μm thickness, similar to so called photonic crystals.[23–25] On the one hand, the array is much thicker than the films, thus the "effective" average grain size along luminous flux could be much larger than that of the films and the randomly distributed nanotubes in de-ionized water. On the other hand, the energy band gap of the BNT material might also be modulated by the structure of nanotube arrays.

In conclusion, BNT thin films and nanotubes are synthesized and their optical properties are investigated. The energy band gap of BNT films shifts to longer wavelength with the increase in grain size owing to the increased integrality of crystal lattice. Nevertheless, although the XRD estimated average grain size of the nanotubes is much smaller than that of the films, the energy band gap of nanotubes shifts even further to longer wavelength. This phenomenon is thought to be related to the nanotube geometry. More experiments on different materials and different nanostructures are still needed to reveal the mechanism.

This work was supported by the National Science Foundation (Grant Nos. 50672034 and 50832002), the 973 Project of MOST (Grant Nos. 2006CB921804 and 2009CB929501), NCET-06-0443, and the Jiangsu Natural Science Foundation (Grant No. BK2007128).

[1] O. Auciello, J. F. Scott, and R. Ramesh, Phys. Today **51**, 22 (1998).
[2] J. F. Scott, *Ferroelectric Memories* (Springer, New York, 2000).
[3] C. H. Ahn, K. M. Rabe, and J. M. Triscone, Science **303**, 488 (2004).
[4] M. Dawber, K. M. Rabe, and J. F. Scott, Rev. Mod. Phys. **77**, 1083 (2005).
[5] F. D. Morrison, L. Ramsay, and J. F. Scott, J. Phys.: Condens. Matter **15**, L527 (2003).
[6] F. D. Morrison, Y. Luo, I. Szafraniak, V. Nagarajan, R. B. Wehrspohn, M. Steinhart, J. H. Wendorff, N. D. Zakharov, E. D. Mishina, K. A. Vorotilov, A. S. Sigov, S. Nakabayashi, M. Alexe, R. Ramesh, and J. F. Scott, Rev. Adv. Mater. Sci. **4**, 114 (2003).
[7] Y. Luo, I. Szafraniak, N. D. Zakharov, V. Nagarajan, M. Steinhart, R. B. Wehrspohn, J. H. Wendorff, R. Ramesh, and M. Alexe, Appl. Phys. Lett. **83**, 440 (2003).
[8] W. S. Yun, J. J. Urban, Q. Gu, and H. K. Park, Nano Lett. **2**, 447 (2002).
[9] R. Skomski, J. Phys.: Condens. Matter **15**, R841 (2003).
[10] J. F. Scott, H. J. Fan, S. Kawasaki, J. Banys, M. Ivanov, J. Macutkevic, R. Blinc, V. V. Laguta, P. Cevc, J. S. Liu, and A. Kholkin, Nano Lett. **8**, 4404 (2008).
[11] J. Junquera and P. Ghosez, Nature (London) **422**, 506 (2003).
[12] I. I. Naumov, L. Bellaiche, and H. Fu, Nature (London) **432**, 737 (2004).
[13] M. Alexe, D. Hesse, V. Schmidt, S. Senz, H. J. Fan, M. Zacharias, and U. Gosele, Appl. Phys. Lett. **89**, 172907 (2006).
[14] J. F. Scott, J. Phys.: Condens. Matter **18**, R361 (2006).
[15] J. F. Scott, Science **315**, 954 (2007).
[16] W. Li, J. Ma, C. H. Song, P. Bao, X. M. Lu, J. S. Zhu, and Y. N. Wang, Chin. Phys. Lett. **21**, 544 (2004).
[17] H. Masuda and K. Fukuda, Science **268**, 1466 (1995).
[18] X. S. Wang, J. W. Zhai, L. Y. Zhang, and X. Yao, Infrared Phys. Technol. **40**, 55 (1999).
[19] A. J. C. Wilson, *X-Ray Optics* (Metheu, London, 1949), p. 45.
[20] W. A. Rachinger, J. Sci. Instrum. **25**, 254 (1948).
[21] J. Callway, *Quantum Theory of the Solid State* (Academic, New York, 1974), p. 525.
[22] X. M. Lu, J. S. Zhu, W. Y. Zhang, G. Q. Ma, and Y. N. Wang, Thin Solid Films **274**, 165 (1996).
[23] Y. Luo, I. Szafraniak, V. Nagarajan, R. B. Wehrspohn, M. Steinhart, J. H. Wendorff, N. D. Zakharov, R. Ramesh, and M. Alexe, Integr. Ferroelectr. **59**, 1513 (2003).
[24] J. Choi, Y. Luo, R. B. Wehrspohn, R. Hillerband, J. Schilling, and U. Gosele, J. Appl. Phys. **94**, 4757 (2003).
[25] P. Xu, S. H. Ji, S. N. Zhu, X. Q. Yu, J. Sun, H. T. Wang, J. L. He, Y. Y. Zhu, and N. B. Ming, Phys. Rev. Lett. **93**, 133904 (2004).